ELSEVIER

#### Contents lists available at ScienceDirect

# Molecular Astrophysics

journal homepage: www.elsevier.com/locate/molap



## Research Paper

# Ro-vibrational analysis of SiO in UV-irradiated environments

Ziwei E. Zhang\*,a, R.S. Cumbeeb, P.C. Stancila, G.J. Ferlandc

- <sup>a</sup> Department of Physics and Astronomy and Center for Simulational Physics, University of Georgia, Athens, GA 30602, USA
- <sup>b</sup> NASA Goddard Space Flight Center, Greenbelt, MD 20771, USA
- <sup>c</sup> Department of Physics and Astronomy, University of Kentucky, Lexington, KY 40506, USA



Keywords: ISM: molecules Photodissociation region (PDR) Molecular data Stars: AGB and post-AGB

#### ABSTRACT

SiO emission lines are important probes of chemical processes in diverse astrophysical environments, commonly observed in shocks associated with the outflows of young stellar objects, both low- and high-mass, and in the envelopes of evolved stars. Modelling SiO emission for conditions of non-local thermodynamic equilibrium (NLTE) requires collisional rate coefficients due to  $H_2$ ,  $H_3$ , and  $H_4$  impact, with the first of these of limited availability. Unknown collisional rate coefficients are often estimated from known systems. For the case of SiO- $H_2$ , rate coefficients have previously been adapted from a different collider,  $H_4$ , based on a reduced-mass scaling approach. Here, we construct comprehensive SiO collisional rate coefficients data with multiple colliders ( $H_2$ ,  $H_4$  and  $H_4$ ) and rovibrational transitions up to v=5 and v=1 and v=1 and v=1 approach is used to estimate unknown collisional data. Using RADEX and Cloudy, we investigate the rotational and rovibrational SiO emission in various astrophysical environments, including photodissociation regions (PDR) and the envelope of VY Canis Majoris.

#### 1. Introduction

Being one of the first detected molecules in the interstellar medium (ISM), SiO has been an important probe of physical and chemical processes in warm molecular regions (Wilson et al., 1971; Ziurys et al., 1989). In many astrophysical environments, SiO is highly excited both rotationally and vibrationally. Theoretical non-local thermodynamic equilibrium (NLTE) study of these environments requires data such as collisional rate coefficients and Einstein A values (van Dishoeck, 2017), while high excitation data being of low availability due to either theoretical or experimental limitations. Here we construct comprehensive collisional rate coefficients data for spectral analysis of SiO due to  $\rm H_2$ ,  $\rm H$  and  $\rm He$  collisions, with a reduced-potential scaling method. (Table A1 shows the SiO data update details. See Appendix A for data construction.) With the new data set, we perform a NLTE rovibrational analysis of SiO in various astrophysical conditions.

With recent developments in observation in the infrared and sub-millimeter with *Herschel*, SOFIA, ALMA and the future launch of *JWST*, we're able to have a more detailed view of many sites of interest, such as star formation regions, protoplanetary disks (PPDs), and AGB envelopes. Studies of such environments require knowledge of photo-dissociation regions (PDRs), where SiO is the main gas-phase carrier of Si (Schilke et al., 2001). With *JWST*, we will be able to study the near-

and mid-infrared range, which motivates investigation of molecular vibrational emission (0.6–10  $\mu m$ ). Currently, spectral analyses are limited to lower rotational states of most molecules (Schöier et al., 2005), due to lack of experimental and computational data. Effort has been made to calculate and extrapolate collisional rate coefficients in higher rotational and vibrational states for molecules such as CO and HCN in various environments (Bruderer et al., 2015; Neufeld, 2012).

SiO is the main Si-bearing molecule in dense clouds and emission from SiO is often found to imply warm temperatures due to extreme conditions such as shocks and UV radiation. Dependency on density and temperature for SiO is due to the gas-phase silicon chemical reactions which were discussed in detail previously by Herbst et al. (1989) and Langer and Glassgold (1990).

A PDR is the interface between an H  $\scriptstyle\rm II$  region and a cold molecular region, where gas is mostly neutral but chemical and physical processes are driven by far UV radiation (  $\sim$  8 eV  $< h\nu < 13.6$  eV). The uprising interest of PDRs revolves around star formation regions, AGB envelopes and outflows, PPDs and other UV irradiated environments, extending to more and more diverse and complex objects and regions. Laboratory astrophysicists hold great curiosity on PDRs, as they're ideal to study the interaction between FUV radiation and neutral gas. Throughout the PDR, the SiO abundance varies with extinction, it becomes the dominant gas-phase Si-carrier at higher  $A_{\rm V}$ , typically when

E-mail address: zzwwin@uga.edu (Z.E. Zhang).

<sup>\*</sup> Corresponding author.

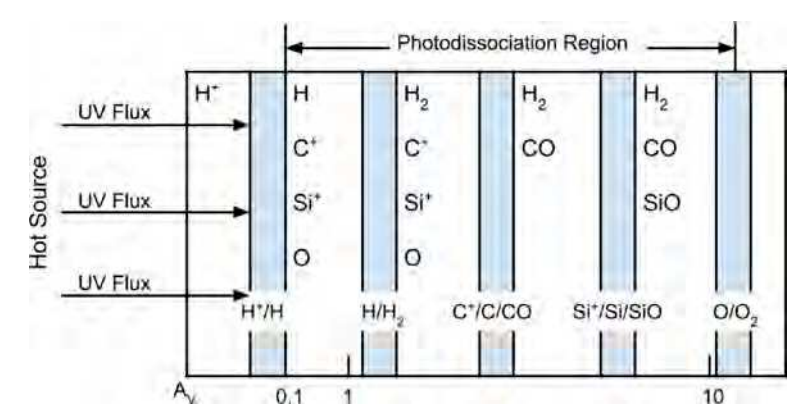


Fig. 1. General PDR structure modified from Hollenbach and Tielens (1999). Hot source on the left irradiates the PDR with UV radiation. CO and SiO are the main gas phase carriers of carbon and silicon.

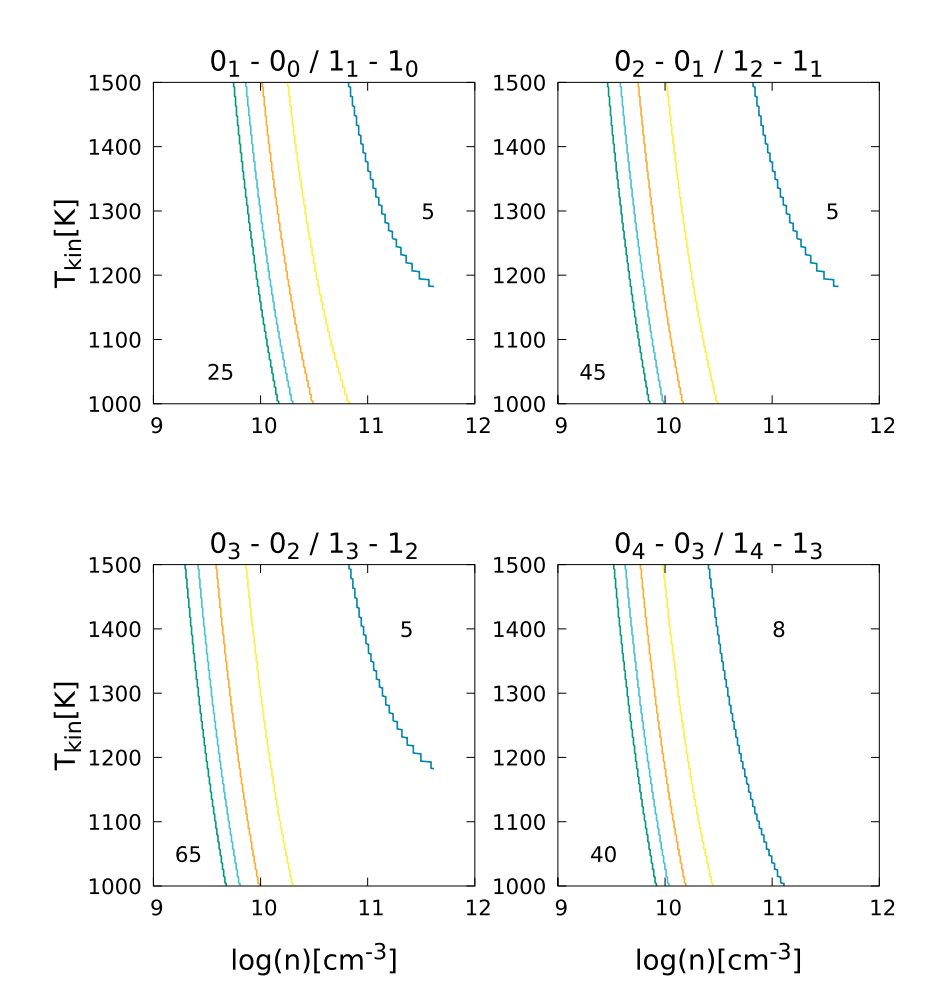


Fig. 2. Diagnostic line ratios ( $\nu = 0/\nu = 1$ ) of SiO rotational transitions in different vibrational states as a function of kinetic temperature and collider density, including  $H_2$ , He and H. (Notation:  $\nu_J$ .) .

 $A_{V}\!>\!6$  (Hollenbach and Tielens, 1999; Sternberg and Dalgarno, 1995; Tielens, 2005). Fig. 1 is a demonstration of the general PDR structure adapted from Hollenbach and Tielens (1999), including silicon species. Recent rapid development in infrared and radio observations has benefited PDR studies, unveiling more details of the ongoing chemical and physical processes.

One of the intriguing aspects of PDR studies is their application to young stellar objects (YSOs), where SiO emission lines play important roles when studying primary and secondary outflows, as well as jets, which are formed in different stages of the YSO evolution (Tan et al.,

2014). They are mostly found in enhanced density regions such as the leading edges of shocks. In the early stage, SiO is often found to be highly collimated along the jets (Arce et al., 2007; Shang et al., 2007). In general, SiO is the best indicator for jets, providing a close-up view when studying molecular outflows around both low- and high-mass YSOs, while other tracers, such as CO, suffer from contamination in swept-up cavities (Leurini et al., 2013). Both low and high rotational transition lines have been observed in massive star formation regions such as Orion KL for J=1-0 and J=2-1, J=8-7 (Beuther et al., 2005), IRAS 17233-3606 (Leurini et al., 2013) for J=5-4 and J=8-7

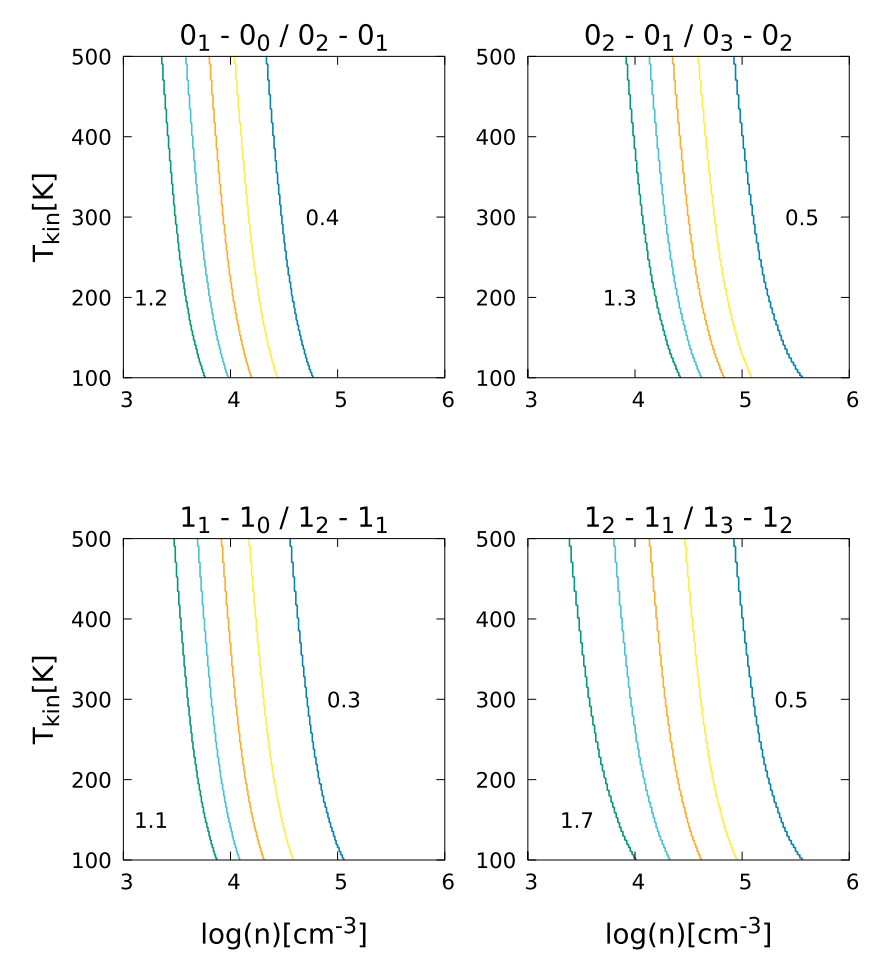


Fig. 3. Diagnostic line ratios of SiO rotational transitions in same vibrational states as a function of kinetic temperature and collider density, including  $H_2$ ,  $H_2$  and  $H_3$ . (Notation:  $\nu_{I^*}$ ).

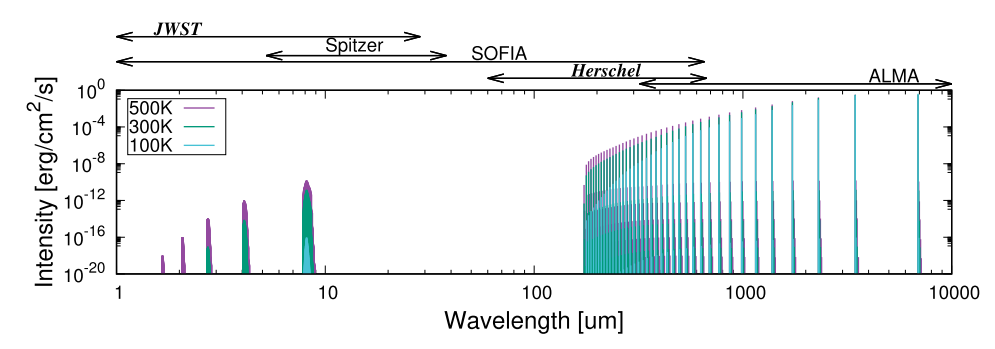


Fig. 4. SiO full line spectra with collider ( $H_2$ , H and He) density of  $10^4$  cm<sup>-3</sup> at 100 K, 300 K and 500 K (indicated with colors). Telescope wavelength coverages are marked on the top.

and the high-mass protocluster NGC 2264-C (López-Sepulcre et al., 2016). With high temperature and density, SiO masers could also be formed in extremely high velocity protostellar winds close to the protostar (Glassgold et al., 1989). Previous studies mainly suggested SiO is an ideal tracer for protostellar activity (Nguyen-Luöng et al., 2013; Nisini et al., 2007; van Dishoeck and Blake, 1998).

AGB stars are of great interest on the other end of the stellar lifecycle, considering they're main producers of dust grains and contribute largely to near-infrared emission in the galaxy. The study of AGB stars is important for understanding dust composition and evolution in general, as well as chemistry related to grains. SiO is one of the signature molecules detected in O-rich AGB stellar envelopes. In the recent study on O-rich AGB stars with <code>Herchel/HIFI</code>, highly excited rotational emission

lines from vibrationaly excited levels for different molecules are detected, with the highest transitions of SiO up to v=1,J=15-14 and v=1,J=23-22 in R Dor and W Hya (Justtanont et al., 2012). For the case of IK Tauri, one of the most investigated O-rich AGB stars, recent studies suggested SiO is depleted in the envelope, likely related to dust formation (Gobrecht et al., 2016). It is also expected to be highly excited near the source, right after it was formed, which makes it a good probe of near-photospheric activity. (Decin et al., 2010; Gobrecht et al., 2016). Meanwhile, SiO holds a key position in studying dust formation in AGB envelopes: silicates start forming from gas-phase SiO and other components at  $\sim 1000$  K (Millar, 2016; van de Sande et al., 2015). However, the near infrared region for AGB stars has not been well studied so far due to either limited observational resolution or lack of

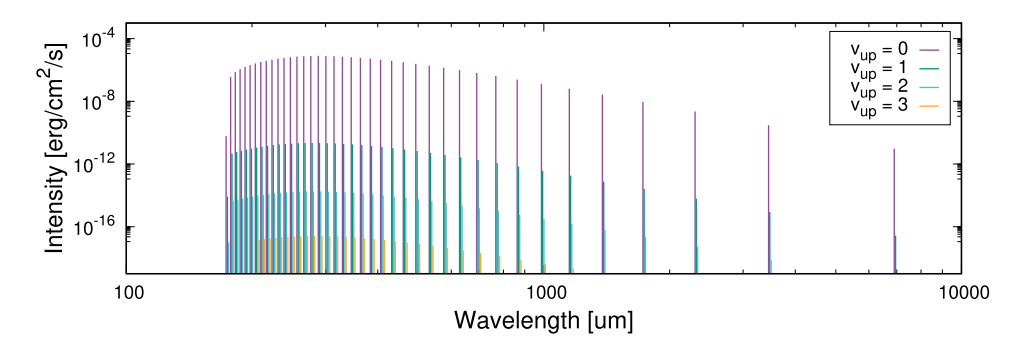


Fig. 5. SiO pure rotational spectrum with a total collider (H2, H and He) density of 108 cm<sup>-3</sup> at 300 K, different vibrational states indicated by color.

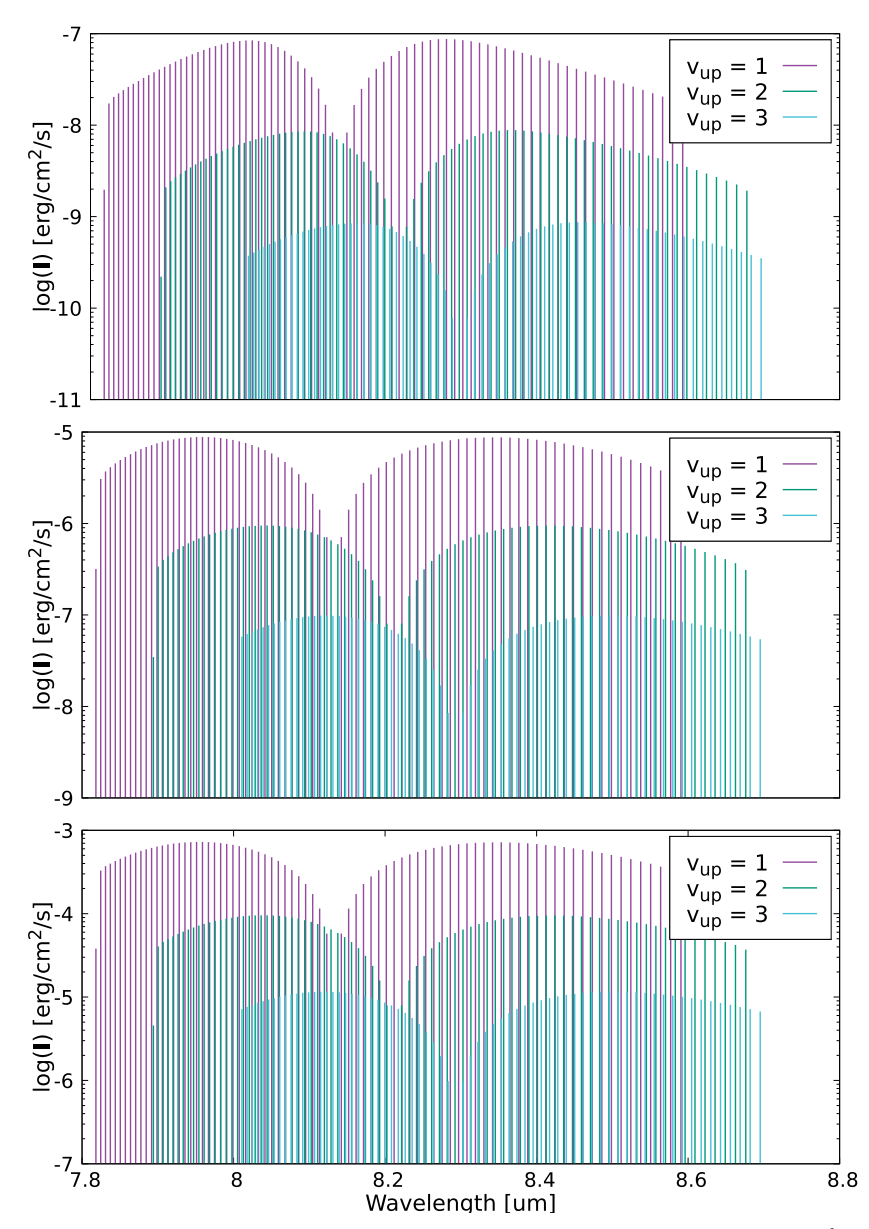


Fig. 6. SiO ro-vibrational spectrum for 1000 K, fundamental band ( $\Delta \nu = -1$ ), with total collider (H<sub>2</sub>, H and He) density of  $10^6$  cm<sup>-3</sup> (top),  $10^8$  cm<sup>-3</sup> (middle) and  $10^{10}$  cm<sup>-3</sup> (bottom). Different upper states are indicated by colors.

**Table 1** PDR Cloudy models with different physical parameters. <sup>a</sup>.

Model	Geometry	$n \text{ (cm}^{-3}\text{)}$ (Density)	$T_{gas}$ (K)	$T_{grain}$ (K)	РАН	$\chi$ $^{ m b}$ (FUV Field)
f1	Semi-infinite,	10 <sup>3</sup>	50	20	No	10
f2	Plane-parallel	$10^{3}$				$10^{5}$
f3	-	$10^{5.5}$				10
f4		10 <sup>5.5</sup>				$10^{5}$
v1	Semi-infinite,	$10^{3}$	Variable,	Variable,	Yes	10
v2	Plane-parallel	$10^{3}$	Self-consistent	Self-consistent		$10^{5}$
v3		$10^{5.5}$				10
v4		$10^{5.5}$				$10^{5}$

<sup>&</sup>lt;sup>a</sup> For more details, see Röllig et al. (2007) and Ferland et al. (2017).

 $<sup>^{\</sup>rm b}~G_0=1.71\chi$ 

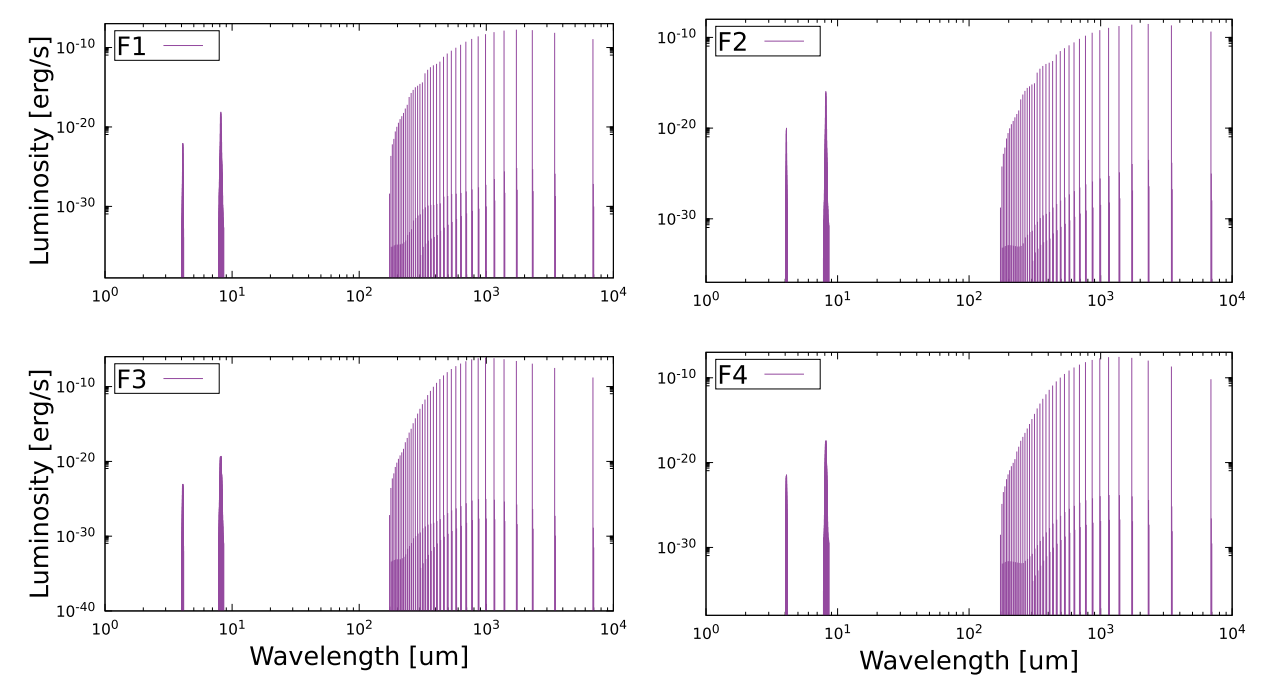


Fig. 7. Full SiO line spectrum for Leiden F Models.

data for vibrational transitions. One of the goals of *JWST* is to study evolved stars, namely AGB stars. In this paper, we attempt a spectral analysis including highly excited rovibrational transitions in both near-and mid-infrared bands for the O-rich AGB star, VY Canis Majoris.

Here we use RADEX (van der Tak et al., 2007) and Cloudy (Ferland et al., 2017) to analyze SiO in warm molecular environments. Both codes utilize molecular collision data in the LAMDA database (Schöier et al., 2005). Currently, the SiO LAMDA format data file includes rate coefficients from one collider: H<sub>2</sub>, adapted from He, based on a reduced-mass scaling approach (Dayou and Balanca, 2006). Our newly constructed SiO collisional rate coefficients data set (see Appendix A for details) is applied in the investigation of SiO emission and abundance in UV-irradiated regions, such as PDR and AGB star envolopes.

## 2. Modeling

To analyze SiO rovibrational emissions, we first use RADEX (van der Tak et al., 2007) to model simple homogeneous environments, studying relevant quantities such as gas temperature and densities with line ratio diagnostics. With Cloudy (Ferland et al., 2017), we consider more complex environments including various physical and chemical processes. We conduct a comparison study on two sets of Leiden

benchmark PDR models with different conditions for NLTE cases (Röllig et al., 2007). Lastly, we construct a model of the envelope for the well-studied O-rich AGB star, VY Canis Majoris, and compare modelling results with observation and other theoretical analysis (Matsuura et al., 2013).

# 2.1. RADEX modeling and results

RADEX is a NLTE radiative transfer code which works with the LAMDA database for a uniform medium, producing level populations and line intensities (van der Tak et al., 2007). Using RADEX, we modelled a uniform sphere with molecular column density of  $10^{12}~\rm cm^{-2}$ , cosmic microwave background (z=0) of 2.73 K and turbulent line width of 1.0 km/s. We also assumed an H<sub>2</sub>/H ratio of 1 and an H/He ratio of 10. With these key parameters, we construct diagnostic plots and line spectra to study SiO in a homogeneous environment.

Diagnostic plots are a helpful and simple way to estimate density, temperature and other physical quantities from observed spectral data. Figs. 2 and 3 show line ratio diagnostic plots for different rovibrational transitions of SiO. Fig. 2 demonstrates a set of diagnostic plots with line ratios between the same rotational transitions in different vibrational levels. Notice the line emissions from different vibrational states are

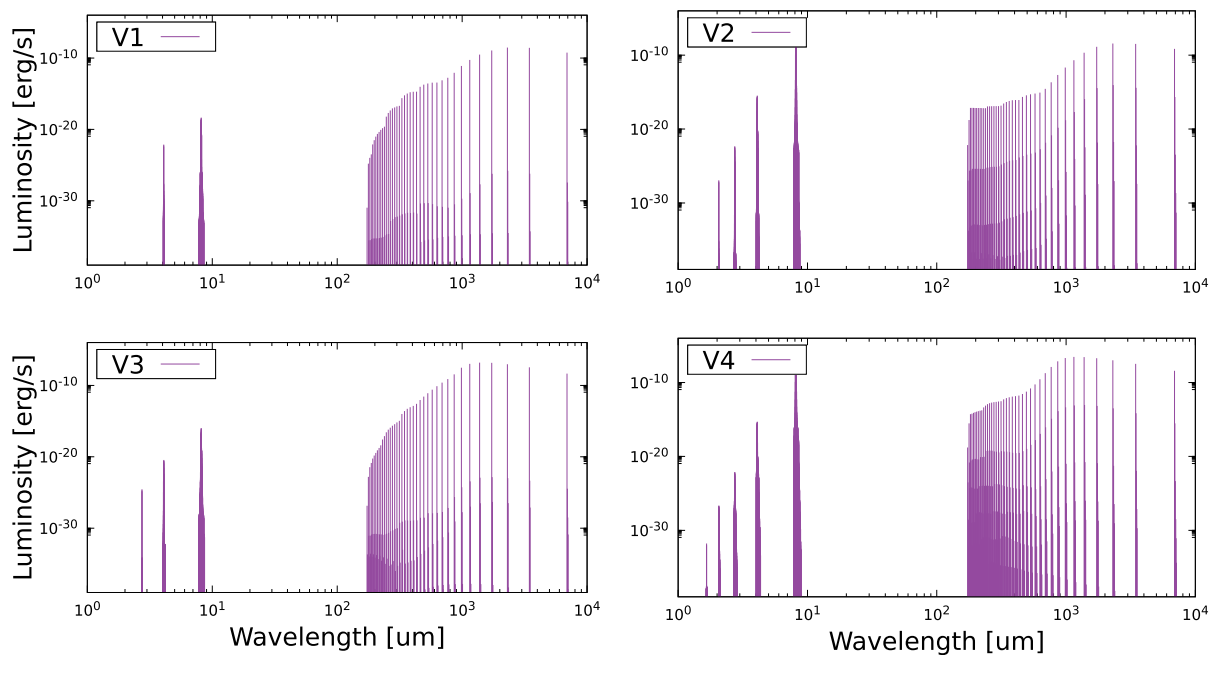


Fig. 8. Full SiO line spectrum for Leiden V Models.

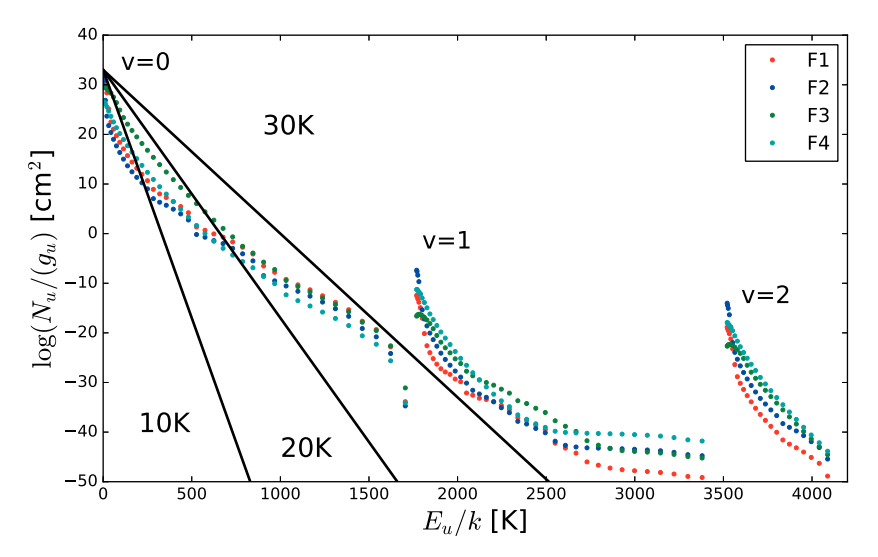


Fig. 9. SiO rotational diagram for Leiden F Models. Solid lines are reference linear fit rotation temperatures.

rather comparable in relatively dense and warm environments, resulting in low line ratios, with higher vibrational levels expected to be more excited. Line ratios are very sensitive to temperature in certain density ranges, making them useful as temperature diagnostics. Fig. 3 is a set of diagnostic plots for the same vibrational levels in a cooler environment. Transitions in the vibration ground state as shown in the top panel while bottom panel shows cases for v = 1. Line ratios between lower and higher level transitions are often around 1, suggesting higher rotational levels are considerably populated in such conditions, which is also indicated in the line spectra shown below. It is possible for masers to be formed with such population inversions (Glassgold et al., 1989). These diagnostic plots would be found most helpful at highly UV irradiated dense cloud surfaces (though we neglect UV radiation in our sample plots). Similar rovibrational diagnostic plots for observed emission lines, such as v = 1, J = 15-14 and v = 1, J = 23-22 observed in R Dor (Justtanont et al., 2012), could be constructed with RADEX for theoretical modelling now with higher vibrational level rate coefficients

available.

We also calculated line spectra to study relative intensities in various environment, shown in Figs. 4-6. Full line spectra as in Fig. 4 compare line emissions at different temperatures at 10<sup>4</sup> cm<sup>-3</sup>. SiO is excited to higher vibrational states in all cases with increasing intensity along with the temperature increase. Observation window for these emission lines are marked at the top panel, extending to near- to midinfrared for vibrational bands. In Fig. 5, in the case of a high collider density of 108 cm<sup>-3</sup> at 300 K, higher rotational excitation are significantly more intense than lower excitation, consistent with diagnostic plot results. Note the cut-off in pure rotational lines near 150  $\mu m$ is due to upper limit of J = 39 in our rotational basis. The fundamental band ( $\Delta v = -1$ ) in warm environments (1000 K) gradually approaches LTE with increasing density as in Fig. 6. Certain lines are relatively intense even for collider density as low as 10<sup>6</sup> cm<sup>-3</sup>, making them good candidates for future mid-infrared observations. The sensitivity with density of these emission lines also suggests related line ratios could be

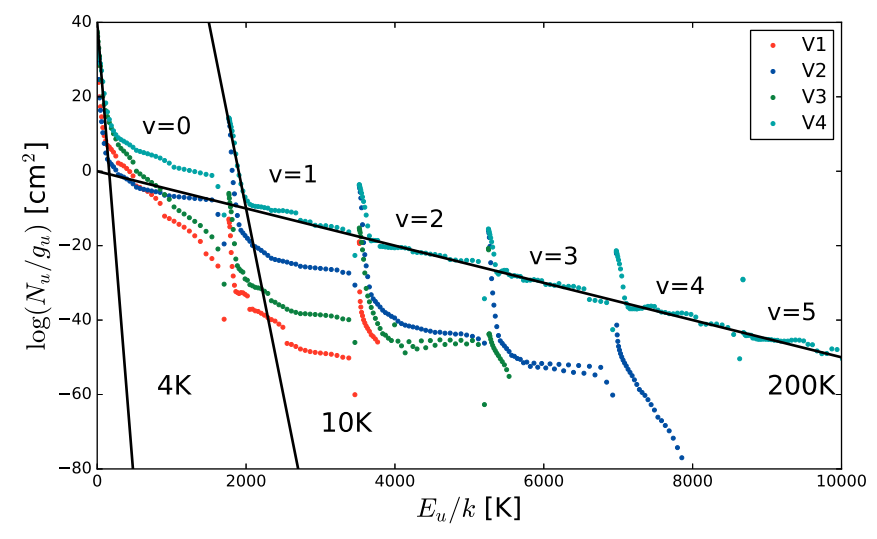


Fig. 10. SiO rotational diagram for Leiden V Models. Solid lines are reference linear fit rotation temperatures.

good diagnostics of density in warm molecular clouds, e.g. PDRs and protoplanetary disks (PPDs).

#### 2.2. Cloudy PDR modelling and results

To simulate more complex conditions in the interstellar medium, we use Cloudy, a spectral synthesis package designed to solve for wide variety of conditions (Ferland et al., 2017). Cloudy has an extensive data system, including the LAMDA, Chianti and Stout databases, which has been continuously updated, for modeling emission and cooling from atoms, molecules, and ions, including radiative transfer effects such as line trapping and pumping. It self-consistently solves for species abundances, ionization balance, and thermal balance including effects due to interstellar dust grains. It also includes various PDR benchmark models (Röllig et al., 2007), giving a range of physical conditions associated with PDR environments. Table 1 lists two sets of related PDR models provided in the Cloudy package and their important distinguishable physical parameters. With these models, we investigate rovibrational SiO emission and other properties in eight representative PDRs, in order to obtain a deeper perception of Si related chemistry and silicate formation. More information regarding chemistry networks and mechanisms could be found in Ferland et al. (2017).

We present a sample of SiO line spectra for the Leiden PDR models as shown in Figs. 7 and 8. In most cases, SiO is excited up to at least  $\nu=2$ , and often as high as  $\nu=5$  (the limit of our database), while pure vibrational transitions in the near-infrared and mid-infrared range have relatively strong emission. Both sets of models share the same trend: high UV radiation and density pump up high rovibrational states. Instead of having constant temperatures as in the F models, V models have self-consistent temperature profiles obtained by solving the heat equation. Source radiation is able to heat up the cloud, thus driving molecules to high rovibrational excitation states throughout the cloud. Such UV-induced high vibrational emissions can be especially seen in V2 and V3 models. It is worth noting that transitions in the fundamental band may be more intense than higher pure rotational transitions, useful when analyzing molecular excitation properties in PDRs.

For sufficiently large density, collisional excitation may drive the molecular level population into LTE. The population for each rovibrational level is given by a Boltzmann distribution (e.g. Goldsmith and Langer, 1999),

$$N_u = \frac{N}{Z} g_u e^{-E_u/kT},\tag{1}$$

which leads to the following:

$$\ln\left(\frac{N_u}{g_u}\right) \propto -\frac{E_u}{kT},\tag{2}$$

where N is the total column density, Z is the rotational and vibrational partition function,  $g_u$  the statistical weight ( $g_u = 2J + 1$ ),  $E_u$  the level energy, k the Boltzmann constant and T the kinetic temperature. Plots for relationship between  $N_u$  and  $E_u$ , the so called rotation diagram, are useful to evaluate excitation and de-excitation and to estimate the kinetic temperature in molecular clouds. However, in NLTE, rotation diagrams present multiple components, rather than a linear trend for the same temperature (e.g. Figs. 9 and 10,  $\nu$  up to 5 and J up to 39). Typically in PDRs, such diagrams show two dominate rotation temperatures for lower Js (lower rotation temperature) and higher Js (much higher rotation temperature) which can be deduced by inverting Eq. (2) to:

$$T_u = \frac{E_u}{k} \ln \left[ \frac{N_u}{N} \frac{Z}{g_u} \right]. \tag{3}$$

For F models, with constant gas temperature, SiO mainly accumulates in the vibrational ground state, showing quasi-LTE behavior. Using a simple linear fit, the kinetic temperatures of 10-30 K could be obtained for F models. A more deliberate method to treat quasi-LTE cases is discussed in Goldsmith and Langer (1999), hence we only show the general population trends and a few reference temperatures here. Multiple components result for V models in Fig. 10, where we give a few reference linear fits. V2 and V4 models present two distinguished temperatures, which represent more realistic PDR environments with the high temperature ( ~ 200K) near the radiation source and the low temperature ( ~ 10 K) further into the cloud. UV radiation partially contributes to high J excitation and drives population up to higher vibrational states. Similar population trends appear throughout different vibrational states due to the dominance of the  $\Delta v = 0$  cascade. The piling-up feature at lower Js is related to the trend of Einstein A coefficients for pure rotational transitions (See Appendix A). It is also possible to deduce a vibration temperature using same J in different vibrational states, which will be explored more in Section 2.3.

To further investigate SiO rovibrational line emission in general PDR environments, we present two sets of continuum spectra for the Leiden PDR models in Figs. 11 and 12. SiO transition lines are marked as dots. Due to the relative low density and temperature, we expected the abundance of SiO to be small due to unfavorable chemistry and high levels of depletion onto dust grains. However, both F and V models show clear SiO rotational lines (zoomed in bottom panel), dominant transitions indicated in the plots are listed in Table 2. Some of these

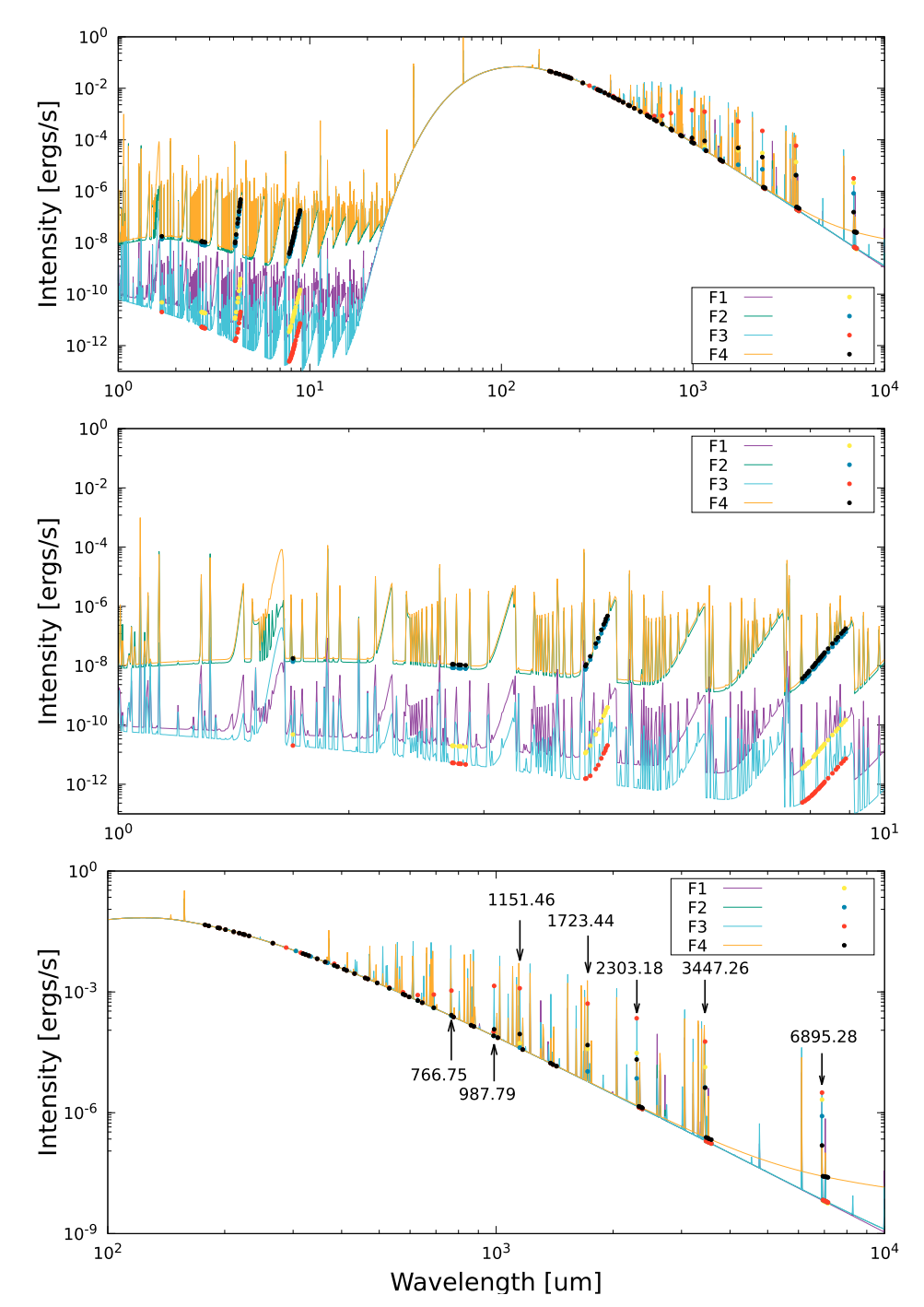


Fig. 11. Continuum spectra for Leiden F models. SiO lines marked as points. Lines indicated (bottom) in rotational spectrum are listed in Table 2.

Table 2
Intense lines in Leiden PDR model continuum.

Wavelength (μm)	Transition $(v', J') \rightarrow (v, J)$
6895.28	$(0, 1) \rightarrow (0, 0)$
3447.26	$(0, 2) \rightarrow (0, 1)$
2303.18	$(0, 3) \rightarrow (0, 2)$
1723.44	$(0, 4) \rightarrow (0, 3)$
1511.46	$(0, 6) \rightarrow (0, 5)$
987.79	$(0,7) \rightarrow (0,6)$
766.75	$(0, 9) \rightarrow (0, 8)$

emission lines, which have intensities a factor of 2–3 above the continuum, are maser candidates. Pure vibrational SiO lines are embedded in  $\rm H_2$  and He continuum (radiative recombination).

With the wide range of astrophysical sources that PDRs are associated with (such as PPDs, AGB stars and star forming regions), these analyses could be implemented in various environments and help to unveil the molecular behaviour.

### 2.3. VY Canis Majoris model with Cloudy

VY Canis Majoris (VY CMa), one the of the brightest AGB stars, has

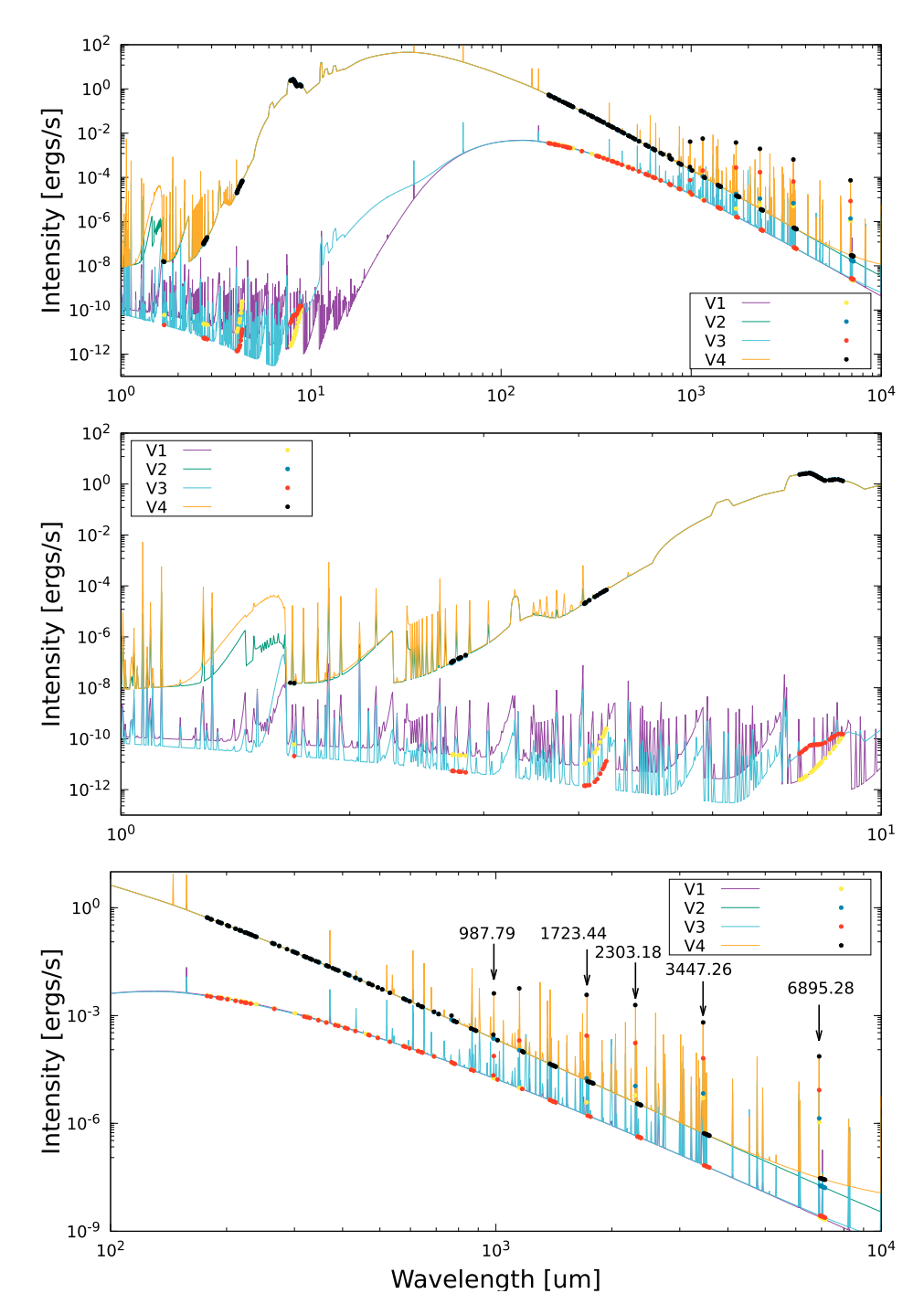


Fig. 12. Continuum spectra for Leiden V models. SiO lines marked as points. Lines indicated (bottom) in rotational spectrum are listed in Table 2.

been very well studied recently (Alcolea et al., 2013; Polehampton et al., 2010; Shenoy et al., 2013). It is one of the earliest SiO maser sources detected. In the past, molecular analysis were only conducted for the vibrational ground states (Matsuura et al., 2013; Richter et al., 2013; 2016; Vlemmings et al., 2017). Higher vibrational state data, not only reveals properties of chemical structure and dust formation in intense conditions such as high radiation and temperature, but is also crucial for maser formation since population inversion is only possible with the existence of higher  $\nu$  states (details discussed in Appendix A).

In the following section, we construct a detailed NLTE circumstellar envelope model for VY CMa, then compare our predictions of the spectral energy distribution (SED) and integrated line intensity with representative previous work from Matsuura et al. (2013), key model

parameters are shown in Table 3 (Matsuura et al., 2013; Wittkowski et al., 2012). We fit the SED to observations as shown in Fig. 13 in order to estimate the dust and chemical composition, as well as other physical conditions. Predicted dust continuum with silicate absorption features (  $\sim$  10, 20  $\mu m$ ) agrees well with the ISO spectrum, while emission lines fit better with Herchel SPIRE spectrum (Matsuura et al., 2013). PACS spectrum (55–190  $\mu m$ ) shows more intense emission than our simulation, suggesting the potential need for rovibrational rate coefficients and NLTE analysis of other molecules that requires higher excitation conditions, such as CO, also not available in the LAMDA database.

As a result of high temperature and density, SiO in VY CMa is almost thermalized, as indicated in Fig. 14. With linear fits, we deduced rotation temperatures for different vibrational states to be  $\sim$  350 K to

**Table 3** Parameters for NLTE VY CMa model<sup>a</sup>.

Model parameters	Values
Geometry & dynamic	Sphere static
R <sub>inner</sub> : Inner radius (cm)	$10^{15}$
R <sub>outer</sub> : Outer radius (cm)	$10^{17.3}$
T: Stellar temperature (K)	3580
•	(Blackbody)
L: Luminosity $(L_{\odot})^{b}$	$2.3 \times 10^{5}$
$n$ : Density $(cm^{-3})^c$	$1.585 \times 10^{9}$
l: Distance (pc)	1170
$d_{min}$ : Minimum dust size (µm)	0.001
$d_{max}$ : Maximum dust size (µm)	0.01
$\Omega_b$ : Estimated beam area (arcsecond <sup>2</sup> )	4

<sup>&</sup>lt;sup>a</sup> Gas-phase chemical abundance: ISM. Dust composition: 10% astronomical silicate and graphite. See more in van Hoof et al. (2004) and Martin and Rouleau (1991).

 $\sim$  550 K with an increasing trend for higher  $\nu$ . We also obtain the vibration temperature for the six vibrational states available in our data, yielding 686 K for J=0,  $\nu=0$ –5. It is expected the vibration and rotation temperature would be approximately the same for full LTE cases, therefore, states within a given  $\nu$  are not in complete LTE. These excitation temperatures are consistent with the range from Matsuura et al. (2013), in which SiO showed two temperature components  $\sim$  1000 K and  $\sim$  200 K.

The species abundances vary throughout the circumstellar envelope as the temperature decreases and dust grains start to form. Hydrogen, carbon and silicon abundance profiles along the envelope are shown in Fig. 15 as a function of physical depth (or radius from the center of the star)  $(10^{15}-10^{17.3}$  cm). Molecule abundances decrease following the -2 density power law, while SiO is depleted significantly around  $10^{15.8}$  cm, where dust condensation and non-equilibrium chemistry set in.

Fig. 16displays the rotational line spectral distribution for VY CMa. Line spectral energy distribution are diagrams with integrated line fluxes per statistical weight as a function of initial excitation energy. They're direct ways to demonstrate rovibrational emission intensities and gas excitation properties, while also containing information about departure from thermal equilibrium. The pattern resembles Fig. A.19 for Einstein A coefficients with groups indicating pure rotational transitions and vibrational transitions of respective  $\Delta v$ . Rotational transitions in the vibrational ground state is shown in the bottom panel of

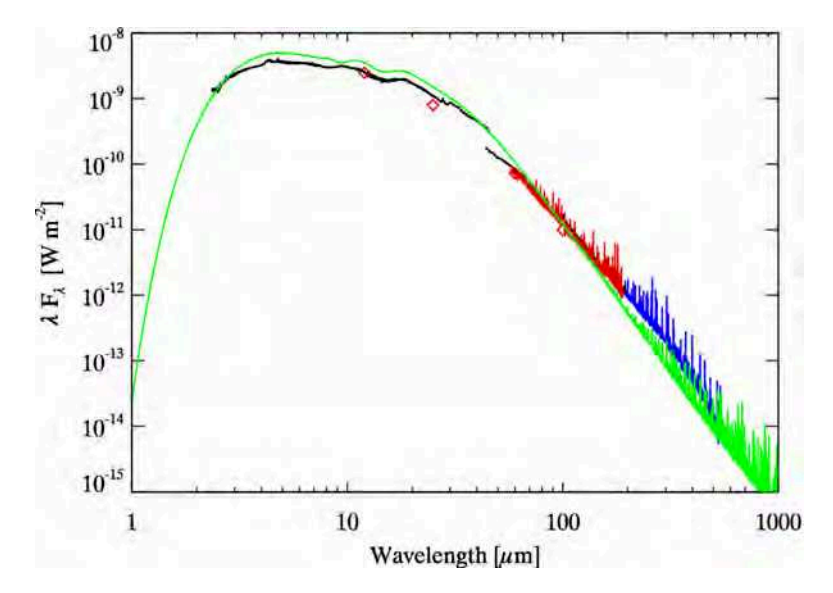


Fig. 16, with observational data marked as diamonds. The Cloudy prediction gives a better agreement at higher excitation than for lower J, while both show features of NLTE conditions. The strong lower J observed flux suggest there may be other excitation sources for SiO other than stellar.

#### 3. Conclusion

Collisional rate coefficient data is one of the fundamental parameters for NLTE analysis of irradiated interstellar environments. With the developments of astrophysical modelling, the need for theoretical calculations has been growing in the past few decades. However, there's still a shortage for such data for high rovibrational transitions due to theoretical and experimental limitations. Vibrational transition data are especially needed for UV-irradiated regions, such as circumstellar envelopes and young stellar objects, where molecules are pumped by radiation. Here we enhance the available collisional data for SiO to include: i) three colliders H2, H and He; and ii) vibrational levels, while applying a reliable scaling method for missing rate coefficients. The effects of our comprehensive data are studied for various environments with the spectral simulation codes RADEX and Cloudy. As the collisional data has become more comprehensive, we expect to have a better understanding of SiO, as well as the chemistry and excitation of other molecules in PDRs and other important astrophysical environments.

In single species homogeneous environments with RADEX, we presented line emission evolution with gas property and diagnostic line ratios, showing significant vibrational excitation for high density and temperature cases.

We analyzed SiO emission and population with two sets of Cloudy PDR models. Spectral analysis show higher rovibrational SiO emission and potential masers, showing the advantage of including higher vibrational levels in our comprehensive data. F models with constant temperature show quasi-LTE behaviour in rotation diagrams, while V models with self-consistent temperature profile show two main temperature components (typical for PDRs).

Another advantage with rovibrational data is in studying highly excited environments, such as the circumstellar envelope for AGB stars. Our model for VY CMa suggests SiO rovibrational levels are highly populated and excited throughout the entire envelope, approaching LTE, with both spectral and level population analysis. Our predicted SED fits previous observation well, while rotation diagram shows consistent excitation temperatures. More detailed modelling and higher resolved observation are needed to reveal the precise structure and composition, as well as molecular excitation and dust formation properties.

Fig. 13. The infrared SED of VY CMa with observations from Matsuura et al. (2013), including SPIRE FTS spectrum (blue), PACS spectrum (red), ISO spectrum (Polehampton et al., 2010; Sloan et al., 2003) (black) and IRAS point source catalogue fluxes (Beichman et al., 1988) (red diamonds). Best-fit model with Cloudy spectrum is shown in green. (For interpretation of the references to color in this figure legend, the reader is referred to the web version of this article.)

<sup>&</sup>lt;sup>b</sup> Power law index: −2.5 for ratio 1 at 0.02 Ryd.

c Power law index: -2.

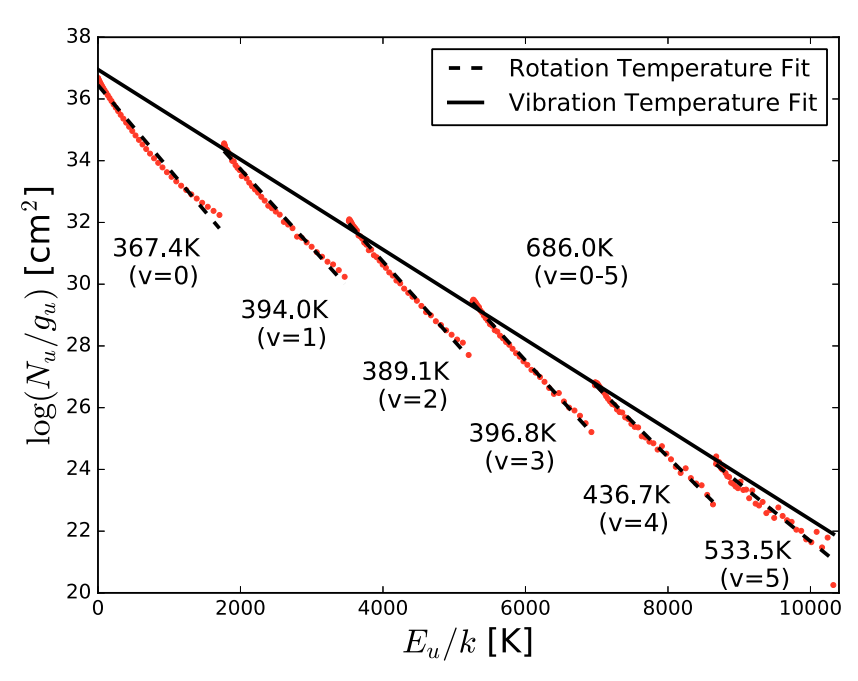


Fig. 14. SiO rotation diagram for VY CMa, rotation and vibration temperatures are deduced with linear fits as indicated.

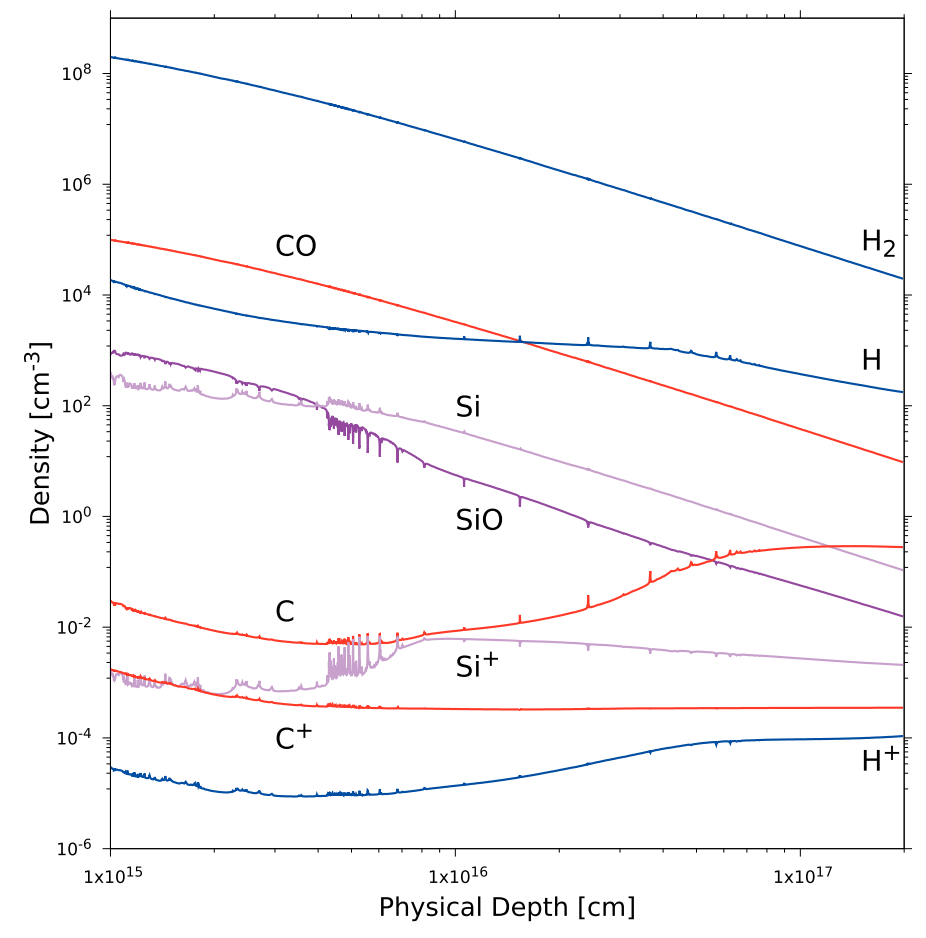
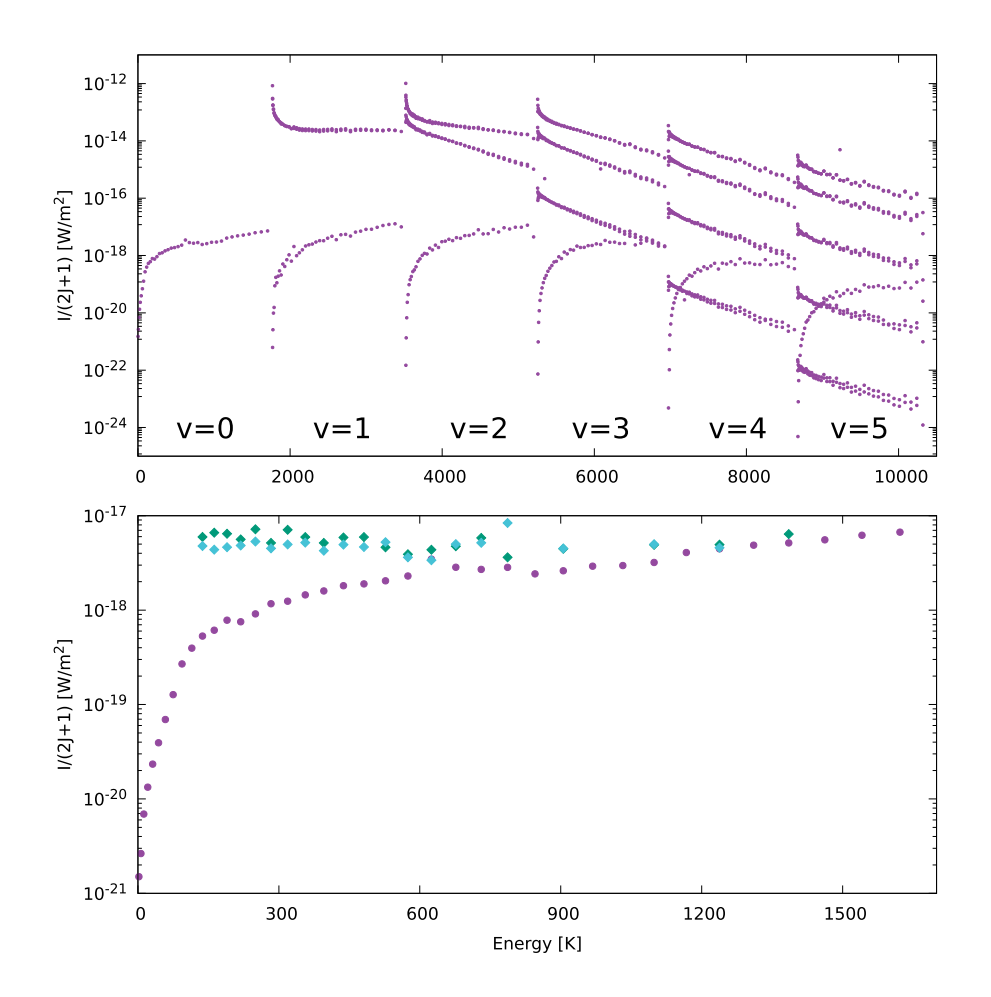


Fig. 15. Species abundances as a function of physical depth in VY CMa, radiation source on the left.



**Fig. 16.** Line spectral energy distribution for VY CMa for v = 0–5, J = 0–39 (top) and vibrational ground state (bottom). Herschel SPIRE data marked as diamonds for two different observations: OD 123 (green) and OD 317 (blue) (Matsuura et al., 2013). (For interpretation of the references to color in this figure legend, the reader is referred to the web version of this article.)

Our predicted results show promising applications for future NIR to submm observation and related exploration. Explicit  $SiO-H_2$  collisional calculations are in progress (Yang et al., 2018) as the current work uses a reduced-potential scaling method to deduce the rate coefficients from SiO-H and -He data. In the near future, we expect to apply rovibrational rate coefficients data for other molecules, including CO, CS and CN, to get a better understanding of the structure and properties UV-irradiated regions.

### Acknowledgements

This work was partially supported by NASA grants NNX12AF42G and NNX15AI61G. We thank Dr. A. P. Palov, Dr. F. Dayou, Dr. C. Balanca, Dr. B. Yang, Dr. F. L. Schöier and Dr. E. J. Barton for providing their data.

#### Appendix A. Rovibrational SiO data construction

Rovibrational analysis for SiO with RADEX and Cloudy requires the collisional rate coefficients in LAMDA data format (Schöier et al., 2005). The current LAMDA database includes pure rotational SiO data obtained with a reduced-mass scaling approach from He (Dayou and Balanca, 2006; Schöier et al., 2005). Recently it's been suggested that scaling via the interaction potential energy surface (PES) well-depth and the reduced masses of

**Table A4**Rovibrational SiO data summary.

Data	Colliders	J	v
SiO-H <sub>2</sub> LAMDA data (Reduced-mass scaling)	$H_2$	0–40	0
SiO data updated	$\mathbf{H}^{\mathrm{a}}$	0-39	0-5
(Reduced-potential method)	$H_2^{\ b}$	0–39	0-5
	He <sup>c</sup>	0–39	0–5

<sup>&</sup>lt;sup>a</sup> Palov et al. (2006, 2002).

 $<sup>^{\</sup>rm b} \ \nu = 0$  data scaled from SiO-He with reduced-potential method,  $\nu = 1-5$  data scaled from SiO-H with reduced-potential method.

 $<sup>^{\</sup>rm c}$   $\nu=0$  data retrieved from LAMDA database (Dayou and Balanca, 2006; Schöier et al., 2005),  $\nu=1-5$  data scaled from SiO-H with reduced-potential method and high temperature data from Balanca and Dayou (2017).

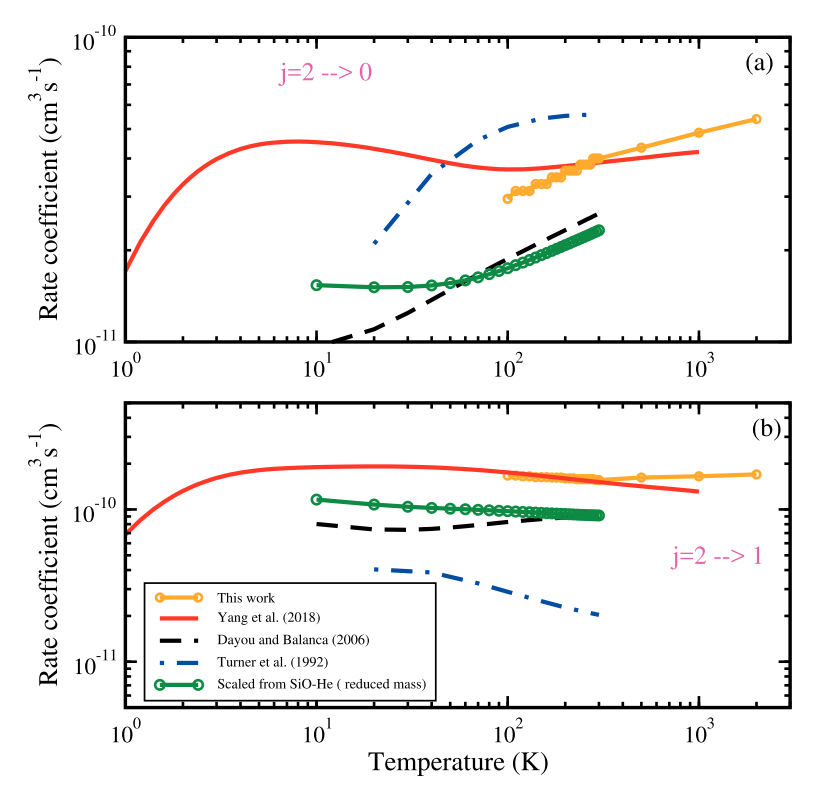


Fig. A17. Comparison of SiO-H<sub>2</sub> data ( $\nu = 0$ ,  $J = 2 \rightarrow 0$  and  $\nu = 0$ ,  $J = 2 \rightarrow 1$ ) in this work using reduced-potential scaling with theoretical calculations from Yang et al. (2018), Dayou and Balanca (2006), Turner et al. (1992) and reduced-mass scaling data (Schöier et al., 2005).

the collisional systems (as shown in the following suggested function) is more reliable (Walker et al., 2014).

$$k_{j\to j'}^Z(T) = \left(\frac{\mu_Z \varepsilon_Z}{\mu_Y \varepsilon_Y}\right)^C k_{j\to j'}^Y(T). \tag{A.1}$$

Here,  $\mu$  is the reduced mass and  $\epsilon$  the van der Waals well depth of the potential energy surface. For SiO,  $\epsilon_{H_2} \approx 293$  (Yang et al., 2018),  $\epsilon_{He} \approx 26.596$  (Dayou and Balanca, 2006),  $\epsilon_H \approx 11$ , 157 cm<sup>-1</sup> (Jimeno, 1999) and we take C = 0.5.

Based on the SiO-H calculations (v = 0 - 5, J = 0 - 39) from Palov et al. (2006, 2002) and original SiO-H<sub>2</sub> LAMDA data file (v = 0, J = 0 - 40), we construct comprehensive rovibrational collisional rate coefficient data set (summarized in Table A.4). SiO-He rovibrational rate coefficients are obtained by, 1) retrieving v = 0 data from LAMDA database (reduced-mass approach with a factor of 1.38) (Dayou and Balanca, 2006; Schöier et al., 2005), 2) scaling v = 1 - 5 SiO-H data (Palov et al., 2006; 2002) with reduced-potential method and 3) including high temperature data from Balanca and Dayou (2017). We also apply reduced-potential scaling method to SiO-He (v = 0) and -H (v = 1 - 5) data to estimate SiO-H<sub>2</sub> rate coefficients.

In Figs. A.17 and A.18, we compare SiO-H<sub>2</sub> data from reduced-potential scaling method in this work with recent theoretical calculation from Yang et al. (2018), as well as from Dayou and Balanca (2006) and Turner et al. (1992) and reduced-mass scaling data (Schöier et al., 2005) in the original LAMDA file. Reduced-potential scaling data presents good agreement with state-of-the-art calculations, thus showing the validity of such method.

Einstein A coefficients adapted from Barton et al. (2013) are shown in Fig. A.19. For the vibrational ground state, A values increase with J. It is unlikely for population inversion to occur with only v = 0 states present, making it impossible for radiative transfer analysis for SiO masers using previous data. The peaks around lower Js indicate pure vibrational transitions at these states are quite probable, leading to the same trend of piling-up effects in the NLTE rotation diagrams (Leiden F and V models).

The complete LAMDA data file is available on the UGA molecular excitation database.

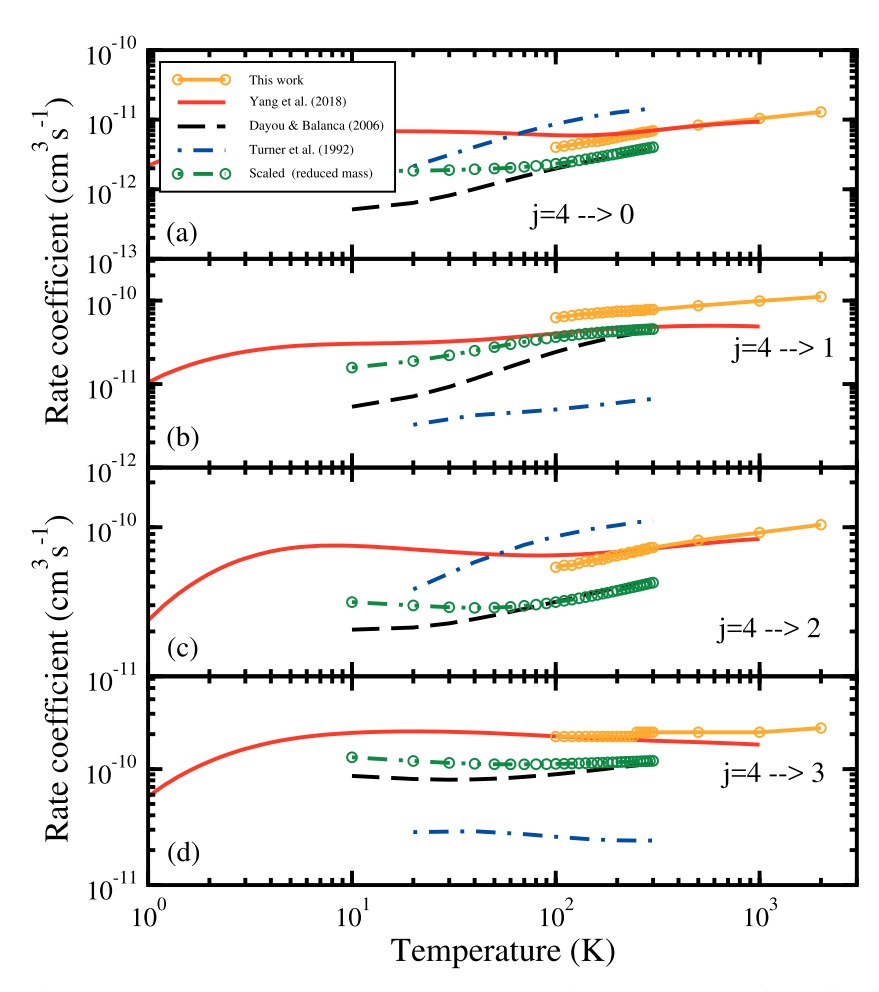


Fig. A18. Comparison of SiO-H<sub>2</sub> data (v = 0,  $J = 4 \rightarrow 0$ , v = 0,  $J = 4 \rightarrow 1$ , v = 0,  $J = 4 \rightarrow 2$  and v = 0,  $J = 4 \rightarrow 3$ ) in this work with theoretical calculations from Yang et al. (2018), Dayou and Balanca (2006), Turner et al. (1992) and reduced-mass scaling data (Schöier et al., 2005).

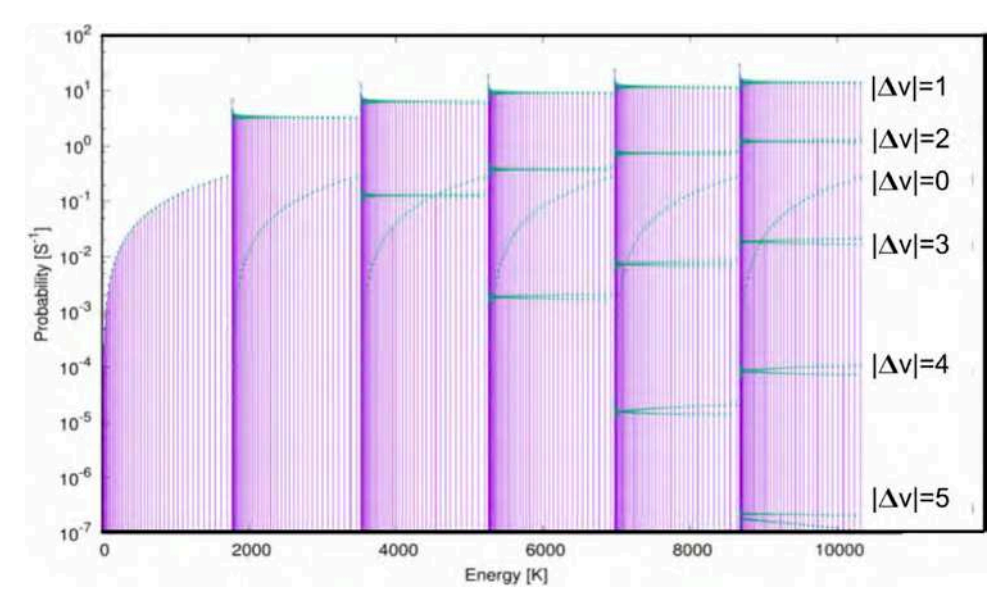


Fig. A19. Einstein A coefficients as a function of upper level energy adapted from Barton et al. (2013), transitions marked with green points. (For interpretation of the references to color in this figure legend, the reader is referred to the web version of this article.)

#### Supplementary material

Supplementary material associated with this article can be found, in the online version, at 10.1016/j.molap.2018.09.001

#### References

- Alcolea, J., Bujarrabal, V., Planesas, P., Teyssier, D., Cernicharo, J., De Beck, E., Decin, L., Dominik, C., Justtanont, K., de Koter, A., Marston, A.P., Melnick, G., Menten, K.M., Neufeld, D.A., Olofsson, H., Schmidt, M., Schöier, F.L., Szczerba, R., Waters, L.B.F.M., 2013. HIFISTARS Herschel/HIFI observations of VY canis majoris. molecular-line inventory of the envelope around the largest known star. Astronom. Astrophys. 559, A93. https://doi.org/10.1051/0004-6361/201321683.
- Arce, H.G., Shepherd, D., Gueth, F., Lee, C.-F., Bachiller, R., Rosen, A., Beuther, H., 2007.
  Molecular outflows in low- and high-Mass star-forming regions. Protostars Planets V 245–260.
- Balanca, C., Dayou, F., 2017. Ro-vibrational excitation of sio by collision with helium at high temperature. Mon. Not. R. Astron. Soc. 469 (2), 1673–1681. https://doi.org/10. 1093/mnras/stx925.
- Barton, E.J., Yurchenko, S.N., Tennyson, J., 2013. Exomol line lists ii. The ro-vibrational spectrum of sio. Mon. Not. R. Astron. Soc. 434 (2), 1469. https://doi.org/10.1093/ mnras/stt1105
- Beichman, C.A., Neugebauer, G., Habing, H.J., Clegg, P.E., Chester, T.J., 1988. Infrared astronomical satellite (IRAS) catalogs and atlases. Volume 1: explanatory supplement. Infrared astronomical satellite (IRAS) catalogs and atlases. 1.
- Beuther, H., Zhang, Q., Greenhill, L.J., Reid, M.J., Wilner, D., Keto, E., Shinnaga, H., Ho, P.T.P., Moran, J.M., Liu, S.-Y., Chang, C.-M., 2005. Line imaging of Orion KL at 865 µm with the submillimeter array. Astrophys. J. 632, 355–370. https://doi.org/10.1086/432974.
- Bruderer, S., HarsonoDaniel, van Dishoeck, Ewine F., 2015. Ro-vibrational excitation of an organic molecule (hcn) in protoplanetary disks. Atlantic Sci. Technol. Acad. Press 575, A94. https://doi.org/10.1051/0004-6361/201425009.
- Dayou, F., Balanca, C., 2006. Rotational excitation of sio by collisions with helium. Atlantic Sci. Technol. Acad. Press 459, 297. https://doi.org/10.1051/0004-6361:20065718
- Decin, L., Justtanont, K., De Beck, E., Lombaert, R., de Koter, A., Waters, L.B.F.M., Marston, A.P., Teyssier, D., Schöier, F.L., Bujarrabal, V., Alcolea, J., Cernicharo, J., Dominik, C., Melnick, G., Menten, K., Neufeld, D.A., Olofsson, H., Planesas, P., Schmidt, M., Szczerba, R., de Graauw, T., Helmich, F., Roelfsema, P., Dieleman, P., Morris, P., Gallego, J.D., Díez-González, M.C., Caux, E., 2010. Water content and wind acceleration in the envelope around the oxygen-rich AGB star IK Tauri as seen by Herschel/HIFI. Atlantic Sci. Technol. Acad. Press 521, L4. https://doi.org/10.1051/0004-6361/201015069.
- Ferland, G.J., Chatzikos, M., Guzmán, F., Lykins, M.L., van Hoof, P.A.M., Williams, R.J.R., Abel, N.P., Badnell, N.R., Keenan, F.P., Porter, R.L., Stancil, P.C., 2017. The 2017 release of span style="font-variant: small-caps;"Cloudy. Rev. Mex. Astron. Astr. 53, 385-438
- Glassgold, A.E., Mamon, G.A., Huggins, P.J., 1989. Molecule formation in fast neutral winds from protostars. Astrophys. J. Lett. 336, L29–L31. https://doi.org/10.1086/ 185354
- Gobrecht, D., Cherchneff, I., Sarangi, A., Plane, J.M.C., Bromley, S.T., 2016. Dust formation in the oxygen-rich AGB star IK Tauri. Atlantic Sci. Technol. Acad. Press 585, A6. https://doi.org/10.1051/0004-6361/201425363.
- Goldsmith, P.F., Langer, W.D., 1999. Population diagram analysis of molecular line emission. Astrophys. J. 517, 209–225. https://doi.org/10.1086/307195.
- Herbst, E., Millar, T.J., Wlodek, S., Bohme, D.K., 1989. The chemistry of silicon in dense interstellar clouds. Atlantic Sci. Technol. Acad. Press 222, 205–210.
- Hollenbach, D.J., Tielens, A.G.G.M., 1999. Photodissociation regions in the interstellar medium of galaxies. Rev. Mod. Phys. 71, 173–230. https://doi.org/10.1103/ RevModPhys.71.173.
- van Hoof, P.A.M., Weingartner, J.C., Martin, P.G., Volk, K., Ferland, G.J., 2004. Grain size distributions and photoelectric heating in ionized media. Mon. Not. R. Astron. Soc. 350 (4), 1330–1341. https://doi.org/10.1111/j.1365-2966.2004.07734.x.
- Jimeno, e.a., 1999. J. Chem. Phys. 111, 4966.
- Justtanont, K., Khouri, T., Maercker, M., Alcolea, J., Decin, L., Olofsson, H., Schöier, F.L., Bujarrabal, V., Marston, A.P., Teyssier, D., Cernicharo, J., Dominik, C., de Koter, A., Melnick, G., Menten, K.M., Neufeld, D., Planesas, P., Schmidt, M., Szczerba, R., Waters, R., 2012. Herschel/HIFI observations of O-rich AGB stars: molecular inventory. Atlantic Sci. Technol. Acad. Press 537, A144. https://doi.org/10.1051/ 0004-6361/201117524.
- Langer, W.D., Glassgold, A.E., 1990. Silicon chemistry in interstellar clouds. Astrophys. J. 352, 123–131. https://doi.org/10.1086/168519.
- Leurini, S., Codella, C., Gusdorf, A., Zapata, L., Gómez-Ruiz, A., Testi, L., Pillai, T., 2013. Evidence of a SiO collimated outflow from a massive YSO in IRAS 17233-3606. Atlantic Sci. Technol. Acad. Press 554, A35. https://doi.org/10.1051/0004-6361/ 201118154.
- López-Sepulcre, A., Watanabe, Y., Sakai, N., Furuya, R., Saruwatari, O., Yamamoto, S., 2016. The role of SiO as a tracer of past star-formation events: the case of the high-mass protocluster NGC 2264-C. Astrophys. J. 822, 85. https://doi.org/10.3847/0004-637X/822/2/85.
- Martin, P.G., Rouleau, F., 1991. Extreme ultraviolet opacity with interstellar dust. In: Malina, R.F., Bowyer, S. (Eds.), Extreme Ultraviolet Astronomy, pp. 341.
- Matsuura, M., Yates, J.A., Barlow, M.J., Swinyard, B.M., Royer, P., Cernicharo, J., Decin,

- L., Wesson, R., Polehampton, E.T., Blommaert, J.A.D.L., Groenewegen, M.A.T., Van de Steene, G.C., van Hoof, P.A.M., 2013. Herschel spire and pacs observations of the red supergiant vy cma: analysis of the molecular line spectra. Mon. Not. R. Astron. Soc. 437 (1), 532. https://doi.org/10.1093/mnras/stt1906.
- Millar, T.J., 2016. Chemistry in AGB stars: successes and challenges. Journal of Physics Conference Series. Journal of Physics Conference Series 728. pp. 052001. https://doi. org/10.1088/1742-6596/728/5/052001.
- Neufeld, D.A., 2012. Collisional excitation of far-infrared line emissions from warm interstellar carbon monoxide (co). Astrophys. J. 749 (2), 125.
- Nguyen-Luöng, Q., Motte, F., Carlhoff, P., Louvet, F., Lesaffre, P., Schilke, P., Hill, T., Hennemann, M., Gusdorf, A., Didelon, P., Schneider, N., Bontemps, S., Duarte-Cabral, A., Menten, K.M., Martin, P.G., Wyrowski, F., Bendo, G., Roussel, H., Bernard, J.-P., Bronfman, L., Henning, T., Kramer, C., Heitsch, F., 2013. Low-velocity shocks traced by extended SiO emission along the W43 ridges: witnessing the formation of young massive clusters. Astrophys. J. 775, 88. https://doi.org/10.1088/0004-637X/775/2/88
- Nisini, B., Codella, C., Giannini, T., Santiago Garcia, J., Richer, J.S., Bachiller, R., Tafalla, M., 2007. Warm SiO gas in molecular bullets associated with protostellar outflows. Astronom. Astrophys. 462, 163–172. https://doi.org/10.1051/0004-6361:20065621.
- Palov, A.P., Gray, M.D., Field, D., Balint-Kurti, G.G., 2006. Modeling of the sio circumstellar maser: rate coefficients for the vibrationally-rotationally inelastic scattering of h+sio. Astrophys. J. 639 (1), 204.
- Palov, A.P., Jimeno, P., Gray, M.D., Field, D., Balint-Kurti, G.G., 2002. Vibrationally-rotationally inelastic cross sections for h+sio collisions. J. Chem. Phys. 116 (4), 1388–1396. https://doi.org/10.1063/1.1421071.
- Polehampton, E.T., Menten, K.M., van der Tak, F.F.S., White, G.J., 2010. The ISO long wavelength spectrometer line spectrum of VY Canis Majoris and other oxygen-rich evolved stars. Astronom. Astrophys. 510, A80. https://doi.org/10.1051/0004-6361/ 200913310.
- Richter, L., Kemball, A., Jonas, J., 2013. Simultaneous VLBA polarimetric observations of the v = {1, 2} j = 1-0 and v = 1, j = 2-1 SiO maser emission towards VY CMa: maser morphology and pumping. Mon. Not. R. Astron. Soc. 436, 1708–1720. https://doi.org/10.1093/mnras/stt1686.
- Richter, L., Kemball, A., Jonas, J., 2016. Simultaneous VLBA polarimetric observations of the  $v=\{1,2\}$  j=1-0 and v=1,j=2-1 SiO maser emission towards VY CMa II: component-level polarization analysis. Mon. Not. R. Astron. Soc. 461, 2309–2327. https://doi.org/10.1093/mnras/stw1302.
- Röllig, M., Abel, N.P., Bell, T., Bensch, F., Black, J., Ferland, G.J., Jonkheid, B., Kamp, I., Kaufman, M.J., Le Bourlot, J., Le Petit, F., Meijerink, R., Morata, O., Ossenkopf, V., Roueff, E., Shaw, G., Spaans, M., Sternberg, A., Stutzki, J., Thi, W.-F., van Dishoeck, E.F., van Hoof, P.A.M., Viti, S., Wolfire, M.G., 2007. A photon dominated region code comparison study. Atlantic Sci. Technol. Acad. Press 467, 187–206. https://doi.org/10.1051/0004-6361:20065918.
- Schöier, F.L., van der TakF. F. S., van Dishoeck, E. F., Black, J. H., 2005. An atomic and molecular database for analysis of submillimetre line observations\*\*\*. A&A 432 (1), 369–379. https://doi.org/10.1051/0004-6361:20041729.
- Schilke, P., Pineau des Forêts, G., Walmsley, C.M., Martín-Pintado, J., 2001. Observations of SiO towards photon dominated regions. Astronom. Astrophys. 372, 291–301. https://doi.org/10.1051/0004-6361:20010470.
- Schöier, F.L., van der Tak, F.F.S., van Dishoeck, E.F., Black, J.H., 2005. An atomic and molecular database for analysis of submillimetre line observations. Atlantic Sci. Technol. Acad. Press 432, 369. https://doi.org/10.1051/0004-6361:20041729.
- Shang, H., Li, Z.-Y., Hirano, N., 2007. Jets and bipolar outflows from young stars: theory and observational tests. Protostars Planets V 261–276.
- Shenoy, D.P., Jones, T.J., Humphreys, R.M., Marengo, M., Leisenring, J.M., Nelson, M.J., Wilson, J.C., Skrutskie, M.F., Hinz, P.M., Hoffmann, W.F., Bailey, V., Skemer, A., Rodigas, T., Vaitheeswaran, V., 2013. Adaptive optics imaging of VY Canis Majoris at 2–5 µm with LBT/LMIRCam. Astron. J. 146, 90. https://doi.org/10.1088/0004-6256/146/4/90.
- Sloan, G.C., Kraemer, K.E., Price, S.D., Shipman, R.F., 2003. A uniform database of 2.4–45.4 micron spectra from the infrared space observatory short wavelength spectrometer. Astrophys. J. Suppl. Ser. 147 (2), 379.
- Sternberg, A., Dalgarno, A., 1995. Chemistry in dense photon-dominated regions. Astrophys. J. Suppl. S 99, 565. https://doi.org/10.1086/192198.
- Tan, J.C., Beltrán, M.T., Caselli, P., Fontani, F., Fuente, A., Krumholz, M.R., McKee, C.F., Stolte, A., 2014. Massive star formation. Protostars Planets VI 149–172. https://doi. org/10.2458/azu\_uapress\_9780816531240-ch007.
- Tielens, A.G.G.M., 2005. The Physics and Chemistry of the Interstellar Medium.
  Turner, E.B., Chan, K.-W., Green, S., Lubowich, A.D., 1992. Tests of shock chemistry in ic
  443g. 399, 114–133.
- van de Sande, M., Decin, L., Lombaert, R., Walsh, C., Khouri, T., Li, X., Millar, T.J., 2015. Unraveling the dust formation process in R Dor. EAS Publications Series. EAS Publications Series 71. pp. 255–257. https://doi.org/10.1051/eas/1571057.
- van der Tak, F.F.S., Black, J.H., Schöier, F.L., Jansen, D.J., van Dishoeck, E.F., 2007. A computer program for fast non-LTE analysis of interstellar line spectra. With diagnostic plots to interpret observed line intensity ratios. Atlantic Sci. Technol. Acad. Press 468, 627–635. https://doi.org/10.1051/0004-6361:20066820.
- E.F. van Dishoeck, Astrochemistry: overview and challenges, ArXiv e-prints (2017). van Dishoeck, E.F., Blake, G.A., 1998. Chemical evolution of star-forming regions. Annu.

- Rev. Astron. Astrophys. 36, 317–368. https://doi.org/10.1146/annurev.astro.36.1.
- Vlemmings, W.H.T., Khouri, T., Martí-Vidal, I., Tafoya, D., Baudry, A., Etoka, S., Humphreys, E.M.L., Jones, T.J., Kemball, A., O'Gorman, E., Pérez-Sánchez, A.F., Richards, A.M.S., 2017. Magnetically aligned dust and SiO maser polarisation in the envelope of the red supergiant VY Canis Majoris. Astronom. Astrophys. 603, A92. https://doi.org/10.1051/0004-6361/201730735.
- Walker, K.M., Yang, B.H., Stancil, P.C., 2014. On the validity of collider-mass scaling for molecular rotational excitation. Astrophys. J. 790,96. https://doi.org/10.1088/0004-637X/790/2/96.
- Wilson, R.W., Penzias, A.A., Jefferts, K.B., Kutner, M., Thaddeus, P., 1971. Discovery of interstellar silicon monoxide. Astrophys. J. Lett. 167, L97. https://doi.org/10.1086/

180769

- Wittkowski, M., HauschildtP. H., Arroyo-Torres, B., Marcaide, J. M., 2012. Fundamental properties and atmospheric structure of the red supergiant vy canis majoris based on vlti/amber spectro-interferometry. A&A 540, L12. https://doi.org/10.1051/0004-6361/201219126.
- Yang, B., Zhang, P., Qu, C., Wang, X.H., Stancil, P.C., Bowman, J.M., Balakrishnan, N., McLaughlin, B.M., Forrey, R.C., 2018. Full-dimensional quantum dynamics of sio in collision with h2. J. Phys. Chem. A 122 (6), 1511–1520. https://doi.org/10.1021/ acs.jpca.7b09762. PMID: 29365271
- Ziurys, L.M., Friberg, P., Irvine, W.M., 1989. Interstellar SiO as a tracer of high-temperature chemistry. Astrophys. J. 343, 201–207. https://doi.org/10.1086/167696.